THE ASTROPHYSICAL JOURNAL, 443:L37–L40, 1995 April 10

AMMONIA EMISSION FROM BOW SHOCKS IN THE L1157 OUTFLOW

M. TAFALLA[1] AND R. BACHILLER[2]
Received 1994 December 20; accepted 1995 January 20

ABSTRACT

We present high-resolution ($\approx 5''$) $NH_3(1, 1)$ and $NH_3(3, 3)$ observations toward the blue lobe of the remarkable bipolar outflow L1157. We find that the ammonia emission arises from several compact condensations that are well aligned with IRAS 20386+6751, the origin of the outflow. The gas that emits in ammonia has been strongly affected by the outflow. In addition of having been accelerated, the gas has been heated to temperatures of more than 60–80 K (a factor of 5 with respect to its quiescent value), and its ammonia abundance has been enhanced by more than an order of magnitude. We interpret the ammonia emission as arising from a series of bow shocks along the outflow axis, and although we cannot detect the shocking agent, our observations suggest that it is in the form of a highly collimated jet. The multiplicity of the ammonia peaks along the outflow suggests the jet is episodic, and the emitting source is so reddened, that most likely represents a case of a Class 0 object.

Subject headings: ISM: individual (L1157) — ISM: jets and outflows — shock waves — stars: formation

1. INTRODUCTION

Bipolar outflows from extremely red objects seem to form a class by their own, distinct from that of outflows from more standard young sources (Bachiller & Gómez-González 1992). The outflow excited by the cold [$F_\nu(100\ \mu m)/F_\nu(60\ \mu m) = 4.0$] object IRAS 20386+6751 in L1157 (Umemoto et al. 1992) is an extreme example of that, as despite the low luminosity of its exciting source ($\approx 11\ L_\odot$), it is interacting with the surrounding cloud in a remarkable way. Umemoto et al. have found that the CO emission from L1157 does not peak toward the *IRAS* source, as expected if the gas were heated by the stellar radiation, but it has a strong maximum toward the blue outflow lobe, as if the gas were heated by the interaction with the high velocity flow. Ammonia observations, especially in the (3, 3) transition (Umemoto et al. 1992; Bachiller, Martín-Pintado, & Fuente 1993), confirm there is a real temperature increase in the gas of the blue lobe. This increase is accompanied by a large ($\approx 10^4$) SiO abundance enhancement, that suggests the heating has occurred through shocks, as dust destruction via shocks is the most likely explanation for such an extreme chemical change (Mikami et al. 1992).

The strong shocks in L1157 are not restricted to the blue side, and Bachiller et al. (1993) have found broad $NH_3(3, 3)$ wings toward both the red and blue lobes. This suggests the shocks do not result from a peculiar environment around the blue lobe, but are an intrinsic characteristic of the outflow. In addition, the same authors find detectable (though not as strong) $NH_3(3, 3)$ emission toward other outflows from deeply embedded objects of similar luminosity (L1448 and IRAS 3282), that suggests there is a relation between source redness and $NH_3(3, 3)$ emission.

In this *Letter*, we present high angular resolution ($\approx 5''$) $NH_3(1, 1)$ and $NH_3(3, 3)$ observations of the blue lobe of the L1157 outflow. We interpret the emission as originating from a series of bow shocks excited by a jet. We estimate the temperature and the ammonia abundance of the shocked gas, and we speculate on the possibility that IRAS 20386+6751 is a Class 0 object.

2. OBSERVATIONS

We observed the $NH_3(1, 1)$ and $NH_3(3, 3)$ transitions simultaneously using the VLA of the NRAO[3] in its D configuration on 1994 February 5. For each transition, both polarizations were detected independently and later combined to maximize the sensitivity. The observations consisted of 15 minute integrations toward L1157 interspersed with 3 minute integrations toward 2021+614 to provide phase calibration; the total time of the observation was 10 hours. Integrations on 3C 286 and 3C 48 were done to provide absolute calibration, and two integrations on 3C 84 were used to calibrate the passband. The correlator was set up with a velocity resolution of 0.62 km s^{-1} and a total coverage of 39 km s^{-1} (63 channels) for each polarization and transition.

To estimate whether our interferometer maps lose any flux because of the lack of baselines smaller than the VLA dish diameter (25 m), we synthesized $NH_3(3, 3)$ and $NH_3(1, 1)$ spectra from selected positions using a 40″ beam, and we compared them to Bachiller et al. 100 m telescope spectra at the same positions. The agreement for $NH_3(3, 3)$ was remarkable, indicating that all the flux is recovered by the interferometer. The agreement for $NH_3(1, 1)$ was also very good, except near the *IRAS* source where we found some sidelobes at the velocity of the ambient cloud. These sidelobes are produced by the very extended ambient core, but because of its narrow line (≈ 0.5 km s^{-1}), only two interferometer channels are affected. All the (1, 1) flux at other velocities is recovered by our observations.

3. RESULTS

Figure 1 (Plate L9) shows the maps of $NH_3(3, 3)$ and $NH_3(1, 1)$ emission integrated from -6 to 5 km s^{-1}, the full velocity range with detected signal. The most notable difference between the two maps is the lack of (3, 3) emission around

[1] Harvard-Smithsonian Center for Astrophysics, MS 42, 60 Garden Street, Cambridge, MA 02138; tafalla@cfa.harvard.edu.
[2] Centro Astronómico de Yebes (IGN), Apartado 148, E-19080, Guadalajara, Spain; bachiller@cay.es.

[3] The National Radio Astronomy Observatory is operated by Associated Universities, Inc., under cooperative agreement with the National Science Foundation.

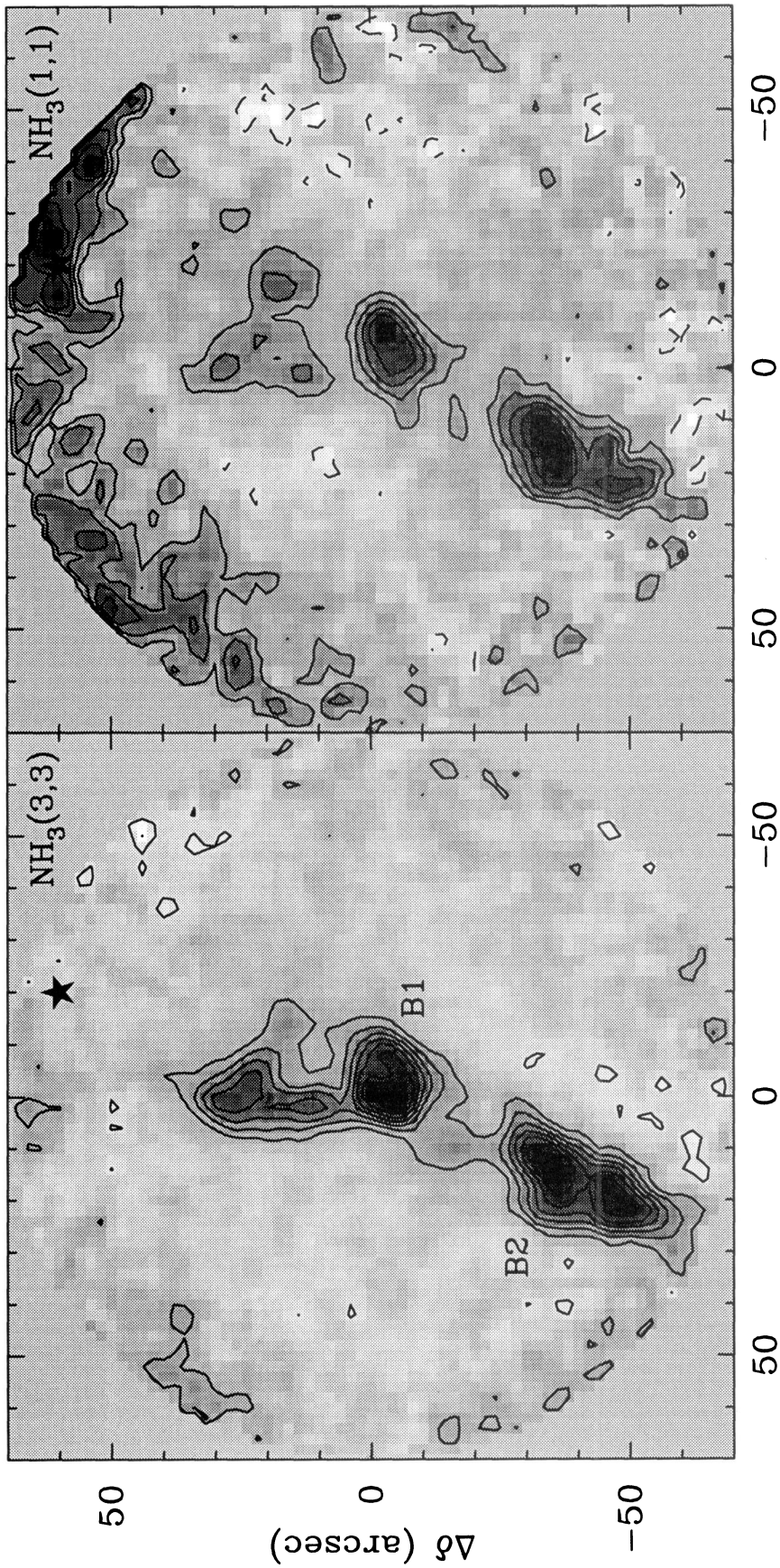

FIG. 1.—Integrated intensity maps of $NH_3(3, 3)$ and $NH_3(1, 1)$ over the interval $-6 < V_{LSR} < 5$ km s^{-1} (*left and right panels*, respectively). The map center is at ($\alpha_{1950} = 20^h38^m43^s.1$, $\delta_{1950} = 67°50'33''$), and the star at ($-20''$, $60''$), represents the position of IRAS 20386+6751. The maps have been corrected for the attenuation of the primary beam of the VLA antennas by dividing them by Gaussians of full width at half-maximum $111''$ (3, 3) and $112''$ (1, 1), and only positions within a radius of $70''$ from the map center are represented. For both maps, the synthesized beam is $5''.8 \times 5''.1$ (P.A. $= -86°$), and the contours are at $\pm 3, \pm 6, \ldots$ K km s^{-1} for $NH_3(3, 3)$ and $\pm 2, \pm 4, \ldots$ K km s^{-1} for $NH_3(1, 1)$.

TAFALLA & BACHILLER (see 443, L37)

the *IRAS* source (represented by a star). This has been previously reported by Bachiller et al. (1993), who separate the ammonia emission into a narrow component, associated with the ambient gas, and a broad component, associated with the outflow. All the (3, 3) emission arises from the broad outflow component, and so does the (1, 1) except in the vicinity of the *IRAS* source. As this narrow emission is strongly affected by the primary beam attenuation, it will not be discussed here, and we will concentrate our attention to the outflow component.

The maps in Figure 1 show that, except for the vicinity of the *IRAS* source, the (3, 3) and (1, 1) emission peak approximately at the same positions, but $NH_3(1, 1)$ is weaker than $NH_3(3, 3)$ by a factor between 2 and 4. The broad ammonia emission arises from two separate condensations approximately aligned with the *IRAS* source. The one at the map center, that will be referred to as B1 (B for "blue"), is rather round and has an extension to the north. It also has a much weaker extension to the northwest, better visible in $NH_3(1, 1)$. The condensation 40″ south of B1 (hereafter B2) is elongated toward the *IRAS* position and has two maxima of similar brightness. Both B1 and B2 lie along the axis of the blue CO outflow mapped by Umemoto et al. (1992), and approximately coincide with the two regions of enhanced CO peak temperature found by these authors. They also coincide with the two relative maxima seen in the low resolution (40″) $NH_3(3, 3)$ map of Bachiller et al. (1993).

The velocity structure of the $NH_3(3, 3)$ emission is presented in Figure 2 in a series of maps at intervals of 1.5 km s^{-1}. [The kinematics of (1, 1) is similar but the emission is weaker.] These maps show that most of the ammonia emission is blueshifted with respect to the ambient cloud (at 2.7 km s^{-1}, see Umemoto et al. 1992), evidencing the emitting gas has been accelerated by the bipolar outflow. B1 dominates the emission at the bluest velocities, while B2 is more concentrated toward the ambient regime. Each condensation shows some, but not much, internal velocity structure. In B1, the main peak dominates at the bluest velocities, while the northern extension brightens at low velocities and becomes almost as prominent as the main peak at about 2 km s^{-1}. The much weaker northwest extension is noticeable in the -2.5 and -1.0 km s^{-1} maps. B2, on the other hand, appears more elongated at the bluest velocities (see 0.5 km s^{-1} map), almost pointing toward the *IRAS* source, and becomes wider, almost triangular, near ambient speeds. The difference in velocity between B1 and B2 is in good agreement with the lower resolution (20″) SiO maps of Mikami et al. (1992), that show the slower emission arises from the gas that is furthest away from the *IRAS* source.

4. DISCUSSION

4.1. *Kinematics of the Emitting Gas*

To study from what type of gas the ammonia emission arises, we present in Figure 3 the $NH_3(1, 1)$ and $NH_3(3, 3)$ spectra from the brightest positions of B1 and B2. In both spectra, the emission peaks near the ambient speed and has a high-velocity wing toward the blue, in good agreement with the spectra from other dense gas tracers like HCO^+, CS, and SiO (Umemoto et al. 1992; Mikami et al. 1992). This spectral shape indicates that the accelerated gas contains a mixture of velocities, and that most of the material is moving at low speeds. Such a distribution cannot arise from moving dense cloudlets ("bullets"), as this would require that most of the gas moves at the cloudlet velocity and little gas remains at low speed. It cannot arise either from condensations like those found in the HH 7–11 outflow by Rudolph & Welch (1988), as those present narrow ($\approx$0.5 km s^{-1}), almost stationary emission.

The mixture of velocities is more suggestive of ambient gas that has been accelerated by a *bow* shock, because in this case

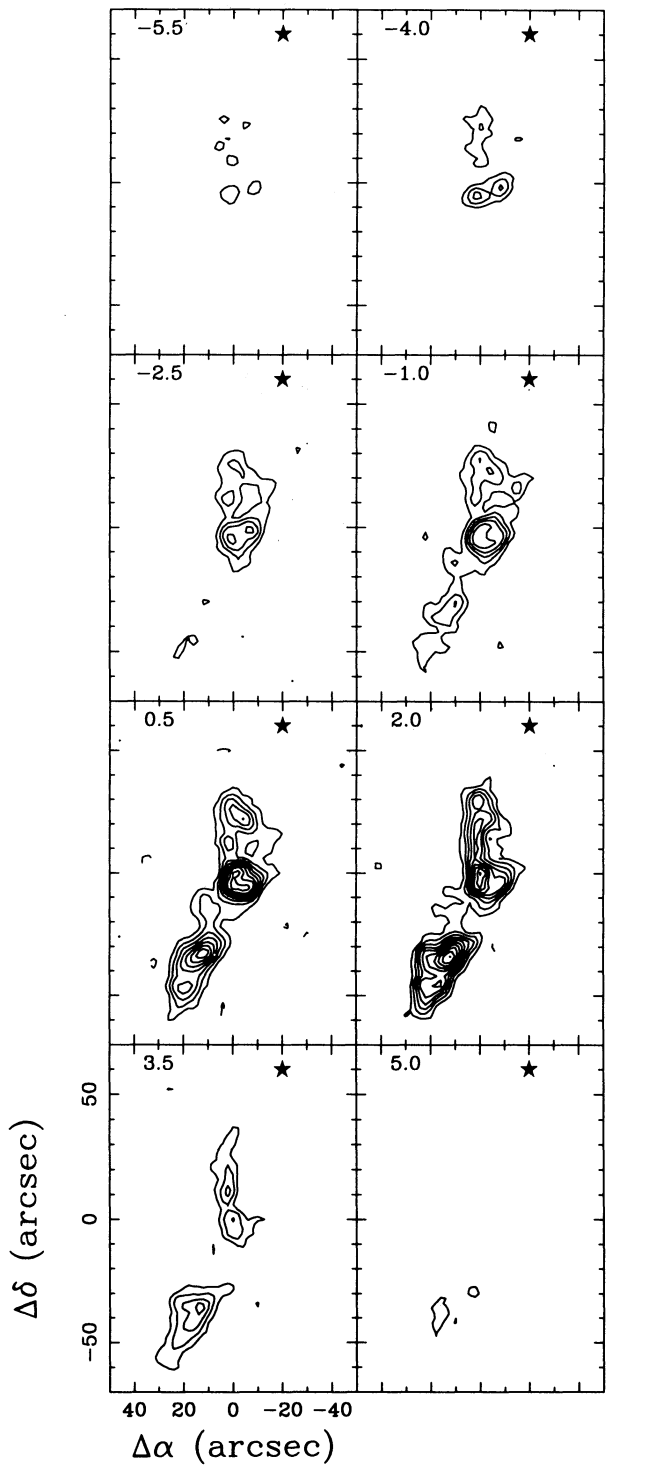

FIG. 2.—Velocity maps of $NH_3(3, 3)$ emission integrated every 1.5 km s^{-1}. Beam size and map center are as in Fig. 1, although no correction for primary beam attenuation has been applied. Contours are at $\pm$0.7, $\pm$1.4, ... K km s^{-1}, and the central velocity of each interval is indicated in the upper left corner of the panel.

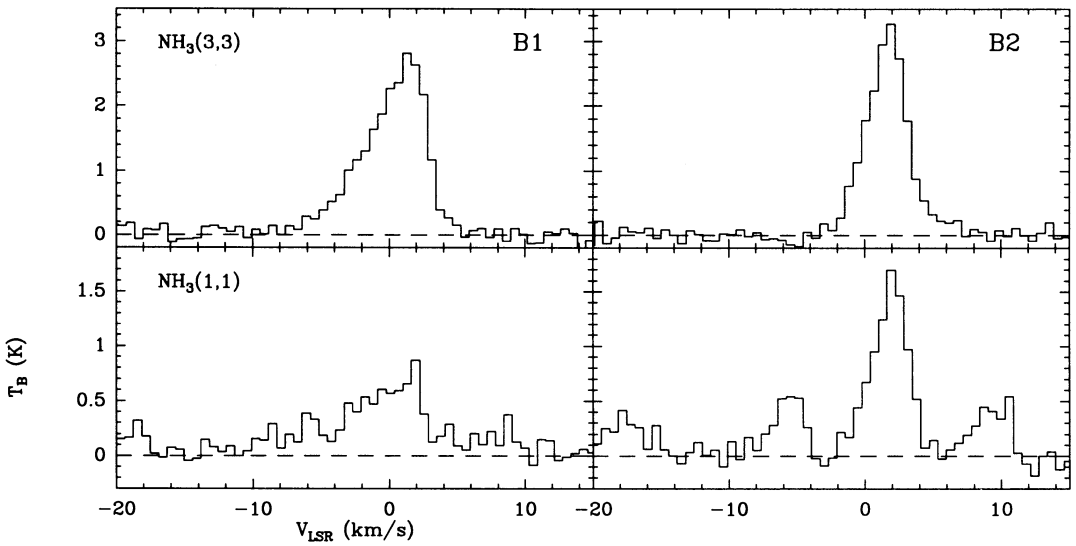

FIG. 3.—$NH_3(3, 3)$ and $NH_3(1, 1)$ spectra toward the brightest positions of B1 and B2. The B1 spectra correspond to position (0, 0) and the B2 spectra to position (15, −35) (offsets are in arcseconds with respect to the same origin as in Fig. 1). In order to enhance their signal-to-noise ratio, the data were convolved with a 10″ beam.

the curvature of a bow shock naturally produces a mixture of accelerations (see, for example, Hartigan, Raymond, & Hartmann 1987; Curiel 1992). This bow shock interpretation is reinforced by the lower velocity of the northern extension of B1, that suggests it originates from a more oblique shock, as expected from that occurring in the wings of a bow shock (see Fig. 2, panels 2.0 and 3.5 km s^{-1}). A comparison of our NH_3 maps with the K' image of Hodapp (1994) further supports this idea. Hodapp's image shows a region of strong diffuse K' emission in the form of a bow near B1, most likely the result of H_2 line emission from a shock. Our ammonia emission, in fact, nicely matches Hodapp's H_2 bow, with the peak of B1 lying near its apex, and the northern and northwest extensions superposed to the sides. A more detailed comparison shows that the $NH_3(3, 3)$ lies about 10″ further away from the *IRAS* source than the H_2. This displacement could result from absorption of the H_2 emission in the inner part of the shock, or from a real stratification of the molecular excitation. More infrared observations are needed to resolve this ambiguity.

4.2. *Kinetic Temperatures*

The kinetic temperature of the shocked gas can be estimated from the ratio between the (3, 3) and (1, 1) intensities. This requires assuming an ortho-to-para abundance ratio, as ammonia molecules in the (3, 3) state belong to ortho-NH_3, while those in the (1, 1) state belong to the para species. Here we assume a ratio equal to the equilibrium value of 2:1 because there is not clear deviation from it in the single-dish data of Bachiller et al. (1993). With this ratio and using the standard equations of the ammonia radiative transfer (see, e.g., Stuzki & Winnewisser 1985) [assuming equal excitation and linewidths for the (3, 3) and (1, 1) transitions], we derive that the ratio of the main component intensities is related to the (1, 1)–(3, 3) rotational temperature (T_{13}) by

$$\frac{I_{33}}{I_{11}} = \frac{1 - e^{-12.5\tau_{11}\, e^{-101/T_{13}}}}{1 - e^{-\tau_{11}}} .$$

As T_{13} is dominated by collisions, it provides a lower limit to the gas kinetic temperature.

To study the spatial distribution of the (3, 3)-to-(1, 1) ratio, and therefore the distribution of gas temperature, we have divided the maps of integrated main component intensity, excluding the two channels with possible contamination by sidelobes from the extended ambient cloud. From the result, we estimate the (3, 3)-to-(1, 1) line ratio varies over the shocked gas from about 1.5 to about 3.5. The highest values are reached toward the northern extension of B1, while the lowest values appear in the northwest extension of the same condensation. B2 has a rather uniform distribution of around 2.2, and the main body of B1 presents values around 3 toward the east and around 2 toward the west. To convert these intensity ratios into T_{13}, we need to estimate the (1, 1) optical depth. This has been done by fitting the (1, 1) profile toward the brightest region (B2, see Fig. 3) using a method similar to that of Pauls et al. (1983). From this fit, we estimate a main component $\tau_{11} = 0.2 \pm 0.2$, that is probably an upper limit for the whole shocked gas, because B2 presents the brightest (1, 1) lines (the spectrum from B1 are too weak to allow a reliable fit). For these low optical depths, T_{13} is almost independent of τ_{11} if $I_{33}/I_{11} < 2$, and is equal to 50 K for a ratio of 1.5. The ratio of 2.2 we find in B2, corresponds to temperatures of the order of 60 K, and the 3.5 ratio from the northern extension of B1 corresponds to 80 K for the optically thin limit, 90 K for $\tau_{11} = 0.1$, and more than 200 K if $\tau_{11} = 0.3$. These temperatures are in good agreement with the single-dish results of Bachiller et al. (1993), who found values between 60 and 100 K from a multiline ammonia analysis. At these large temperatures, the rotational transitions are probably not thermalized (Danby et al. 1988), and the real gas kinetic temperatures may be significantly higher. In any case, even our lower limits already show that there has been an appreciable heating of the gas, as the temperature of the quiescent cloud around the *IRAS* source is only 13 K (Bachiller et al. 1993).

4.3. *Ammonia Abundance Enhancement*

In addition to accelerating and heating, the shock has altered the chemistry of the gas. The SiO abundance has been enhanced by a large factor ($\approx 10^4$), most likely due to grain destruction (Mikami et al. 1992). In these circumstances, we

can expect a simultaneous enhancement of the ammonia abundance, as solid ammonia in grain mantles will either be evaporated at high temperatures, or released when the grains are destroyed. To assess this enhancement, we calculate the NH_3 column density toward B1 and B2, assuming that the (1, 1) transition is optically thin (so our estimates are lower limits) and that the rotation temperature is 70 K (the exact temperature value has little influence on the estimate). By integrating the (1, 1) intensity under the main component, we obtain ammonia column densities of 5.1×10^{14} and 5.4×10^{14} cm^{-2} for B1 and B2, respectively. These column densities are very similar to the 5.2×10^{14} cm^{-2} found by Bachiller et al. (1993) toward the *IRAS* source, and this already indicates that there must be an abundance enhancement of NH_3 toward the shocks, since it is unlikely that given the difference in sizes between the core and the B1 and B2 condensations, the similar NH_3 column densities correspond to similar H_2 column densities. If we use Umemoto et al.'s H_2 column density for the blue outflow at the position of B1 (4×10^{20} cm^{-2}), we derive an ammonia abundance of 1.3×10^{-6}. This is more than an order of magnitude larger than the typical abundances measured in dark clouds (e.g., 3×10^{-8} in IC 348, Bachiller, Guilloteau, & Kahane 1987).

4.4. *Wind Properties*

Although the wind producing the bow shocks cannot be seen directly, some of its properties can be inferred from our observations. The good alignment of B1 and B2 with the *IRAS* source suggests the wind is well collimated. The two peaks of B2, for example, subtend an angle of about 8° from the *IRAS* source, and the only misalignment in all the ammonia emission is caused by the northern extension of B1, that most likely results from the bow shape of the shock. In addition, the lack of $NH_3(3, 3)$ emission toward the *IRAS* source shows the wind flows unimpeded through the dense core despite there is no evidence for any evacuated cavity. All this suggests that the wind is in the form of a jet and, therefore, our observations favor jet driven outflow models, like those of Masson & Chernin (1993), Raga & Cabrit (1993), and Stahler (1993).

The invisible wind probably is also time dependent. B1 and B2 are spatially separated along the outflow enough to be interpreted as two independent bow shocks, and the K' image of Hodapp (1994) confirms that B1 is a fully formed bow shock separated from B2. This configuration of multiple bow shocks along the outflow axis reminds of some optical systems, like HH 34 (Reipurth & Heathcote 1992), and is best explained as resulting from time variations in the driving jet (see, e.g., Raga et al. 1990).

Finally, the shock at B2 seems weaker than at B1. Both Figure 2 and Figure 3 show B2 presents lower velocities than B1, and in addition, there is no shocked H_2 emission toward B2 in Hodapp's image. This weaker shock at B2 could result from the wind slowing down as it moves away from the source and interacts with the molecular gas. It could also result from the ejection episode that gave rise to B2 being weaker, and therefore having less effect on the cloud.

4.5. *The Exciting Source: a Class 0 Object?*

As mentioned before, the L1157 outflow is remarkable in presenting strong $NH_3(3, 3)$ emission from shocked gas despite being powered by a low luminosity source. The other low luminosity sources with detected (3, 3) emission (L1448 and IRAS 3282, Bachiller et al. 1993) are among the most embedded objects known (Class 0; André, Ward-Thompson, & Barsony 1993), and this suggests there is a correlation between (3, 3) emission and source redness. From the *IRAS* fluxes of IRAS 20386+6751 (the only photometry available), we can see that its redness is in fact extreme, comparable to that of other Class 0 objects. The 60 and 100 μm fluxes (10.9 and 43.5 Jy) are very similar to those of B335 (8.3 and 42 Jy, respectively), suggesting IRAS 20386+6751 is a bona fide Class 0 object.

We can only speculate why the youngest outflows produce the striking shocks we observe in $NH_3(3, 3)$. It could be that because of their extreme youth, the stellar wind has not cleared the environment enough, so there is still dense gas in the path of the wind. Or it could be that outflows weaken (or decollimate) as they age, being strong enough to excite NH_3 emission only at their earliest stages. In any case, understanding the peculiarities of the youngest outflows seems a key step in understanding the still mysterious mechanism that drives all bipolar flows.

We thank the staff of the VLA for making possible the observations presented in this *Letter*, and Salvador Curiel for useful conversations on shocks.

REFERENCES

André, P., Ward-Thompson, D., & Barsony, M. 1993, ApJ, 406, 122
Bachiller, R., & Gómez-González, J. 1992, A&AR, 3, 257
Bachiller, R., Guilloteau, S., & Kahane, C. 1987, A&A, 173, 324
Bachiller, R., Martín-Pintado, J., & Fuente, A. 1993, ApJ, 417, L45
Curiel, S. 1992, Ph.D. thesis, Univ. Nacional Autónoma de México
Danby, G., Flower, D. R., Valiron, P., Schilke, P., & Walmsley, C. M. 1988, MNRAS, 235, 229
Hartigan, P., Raymond, J., & Hartmann, L. 1987, ApJ, 316, 323
Hodapp, K. W. 1994, ApJS, 94, 615
Masson, C. R., & Chernin, L. M. 1993, ApJ, 414, 230
Mikami, H., Umemoto, T., Yamamoto, S., & Saito, S. 1992, ApJ, 392, L87
Pauls, T. A., Wilson, T. L., Bieging, J. H., & Martin, R. N. 1983, A&A, 124, 23
Raga, A. C., & Cabrit, S. 1993, A&A, 278, 267
Raga, A. C., Cantó, J., Binette, L., & Calvet, N. 1990, ApJ, 364, 601
Reipurth, B., & Heathcote, S. 1992, A&A, 257, 693
Rudolph, A., & Welch, W. J. 1988, ApJ, 326, L31
Stahler, S. W. 1993, in Astrophysical Jets, ed. M. Livio, C. O'Dea, & D. Burgarella (Cambridge: Cambridge Univ. Press), 183
Stuzki, J., & Winnewisser, G. 1985, A&A, 148, 254
Umemoto, T., Iwata, T., Fukui, Y., Mikami, H., Yamamoto, S., Kameya, O., & Hirano, N. 1992, ApJ, 392, L83